metals

MDPI

Article

Formation and Corrosion Behavior of Mechanically-Alloyed Cu–Zr–Ti Bulk Metallic Glasses

Pee-Yew Lee [1], Yeh-Ming Cheng [1], Jyun-Yu Chen [1] and Chia-Jung Hu [2,*]

[1] Institute of Materials Engineering, National Taiwan Ocean University, Keelung 20224, Taiwan; pylee@ntou.edu.tw (P.-Y.L.); zzz200583815@gmail.com (Y.-M.C.); 10455016@ntou.edu.tw (J.-Y.C.)

[2] Department of Materials Engineering, Tatung University, 40 Chungshan N. Road, 3rd Sec., Taipei 10452, Taiwan

* Correspondence: cjhu@ttu.edu.tw; Tel.: +886-2-2182-2928 (ext. 6228); Fax: +886-2-2593-6897

Academic Editors: Jordi Sort Viñas and K.C. Chan

Received: 31 August 2016; Accepted: 18 April 2017; Published: 20 April 2017

Abstract: $Cu_{60}Zr_{30}Ti_{10}$ metallic glass powder was prepared by mechanically alloying a mixture of pure Cu, Zr, and Ti powders after 5 h of milling. $Cu_{60}Zr_{30}Ti_{10}$ bulk metallic glass (BMG) was synthesized by vacuum hot pressing the as-milled $Cu_{60}Zr_{30}Ti_{10}$ metallic glass powder at 746 K in the pressure range of 0.72–1.20 GPa, and the structure was analyzed through X-ray diffraction and transmission electron microscopy. The pressure could enhance the thermal stability, and prolong the existence, of the amorphous phase inside the $Cu_{60}Zr_{30}Ti_{10}$ powder. Furthermore, the corrosion behavior of the Cu-based BMG in four corrosive media was studied using a potentiodynamic method. The $Cu_{60}Zr_{30}Ti_{10}$ BMG exhibited a low corrosion rate and current density in 1 N solutions of H_2SO_4, NaOH, and HNO_3. X-ray photoelectron spectroscopy results revealed that the formation of Zr- and Ti-rich passive oxide layers provides a high corrosion resistance against 1 N H_2SO_4 and HNO_3 solutions, and the breakdown of the protective film by Cl^- attack was responsible for pitting corrosion in a 3 wt % NaCl solution. The formation of oxide films and the nucleation and growth of pitting were analyzed through microstructural investigations.

Keywords: mechanical alloying; bulk metallic glass; corrosion; supercooled liquid region; vacuum hot pressing

1. Introduction

Recently, new metallic glass alloys with a wide supercooled liquid region exceeding 30 K have been prepared in numerous Cu-based alloy systems, such as Cu–Ti–Zr, Cu–Hf–Ti, Cu–Zr–Hf–Ti, Cu–Zr–Ti–Y, Cu–Ti–Zr–Ni–Si, and Cu–Ti–Zr–Ni–Sn systems [1–3]. Cu-based bulk metallic glasses (BMGs) with diameters ranging from 2 mm to 6 mm have been produced using conventional casting techniques at a low cooling rate [2]. These new alloys are expected to increase the number of application fields of BMGs because of their unique properties, such as high tensile strength, large elastic limits (~2%), and high resistance to corrosion and wear. The defining characteristic of metallic glasses, compared to conventional metallic materials, is their lack of crystallinity, and associated lack of microstructural features, such as grain and phase boundaries [4]. Metallic glasses clearly cannot have the crystallographically-defined slip-systems of polycrystalline metals. In the absence of dislocation-mediated slip, they show high yield stresses, much closer to the theoretical limit than their crystalline counterparts [5]. Therefore, the lack of grain structure and associated microstructural features (e.g., solute segregation) gives corrosion resistance. BMGs exhibited excellent corrosion resistance compared to that of the crystalline alloys. This can be attributed to the beneficial effect of the

alloying components, such as Nb in ZrCuNiAl BMG [6], or Ag, Ni in passive film on the MgCu BMG [7], which are homogeneously mixed in the amorphous phase. Thus far, many researchers have studied the glass-forming ability, thermal stability, and mechanical properties of all of the aforementioned Cu-based BMGs. While BMGs are still little used because of their macroscopic brittle nature and the difficulty of processing, thin film metallic glasses (TFMGs) are a possible solution to take advantage of the unique MG properties of high strength [8,9], large plasticity within ΔT, excellent wear resistance, annealing-induced amorphization, and the resulting smooth surfaces [10]. The lack of ductility is mainly due to the detrimental formation of a few large localized shear bands, leading to the catastrophic fracture [11,12]. There have been several approaches to improve the room temperature ductility in BMGs, including microstructure modification by forming composite structures in the amorphous matrix [13,14], and surface modifications, such as thick (~90 μm) coatings [15]. However, data on the corrosion behavior of Cu-based BMGs and TFMGs are comparatively rare. The application of Cu-based BMGs requires that they have an acceptable lifetime in different environments. Hence, investigating the corrosion behavior of Cu-based metallic glasses in many aggressive environments, such as acidic and salt solutions, at ambient temperatures and in humid air, is of scientific and technological consequence.

A large supercooled liquid region is known to be essential for the formation of BMGs through rapid solidification; however, this restricts BMG formation to near-eutectic compositions, where supercooling can be achieved without the nucleation of crystalline phases. In this regard, an alternative method to prepare metallic glasses is mechanical alloying (MA) [16]. Previous investigations have demonstrated the successful use of MA for synthesizing metallic glass powders with large supercooled regions [17,18]. The existence of a wide supercooled liquid region enables the preparation of BMGs by hot pressing or extruding metallic glass powders at temperatures above the glass transition temperature (T_g) because of the rapidly decreasing viscosity of the metallic glass [19,20]. Therefore, in this study, the feasibility of preparing a $Cu_{60}Zr_{30}Ti_{10}$ BMG by using the MA and vacuum hot pressing techniques was investigated. Furthermore, the corrosion behavior of the $Cu_{60}Zr_{30}Ti_{10}$ BMG in four corrosive media (1 N H_2SO_4, HNO_3, and NaOH and 3 wt % NaCl) was studied using a potentiodynamic method.

2. Experimental Procedure

Elemental powders of Cu (99.9%, <300 mesh), Ti (99.9%, <100 mesh), and Zr (99.9%, <325 mesh), were weighed to yield the desired composition, $Cu_{60}Zr_{30}Ti_{10}$, and then canned into an SKH 9 high-speed steel vial together with Cr steel balls in an argon-filled glove box, where a SPEX 8016 shaker (SPEX SamplePrep, Metuchen, NJ, USA) ball mill was used for MA. The details of the MA process are described elsewhere [21]. The bulk samples were prepared by consolidating the as-milled powder in a vacuum hot pressing machine (Giant-asia, Miaoli, Taiwan) at 746 K under a pressure range of 0.72–1.20 GPa. The structure of the as-milled and bulk samples was analyzed using a Siemens D-5000 X-ray diffractometer (CountrySiemens AG, Karlsruhe, Germany). Thermal analysis was performed using a Dupont 2000 differential scanning calorimeter (DSC, CountryTA instruments, New Castle, PA, USA) at a heating rate of 40 K/min. The corrosion characteristics of the alloys were determined on the basis of anodic polarization curves obtained using a potentiodynamic method. Prior to the corrosion tests, the specimens were mechanically polished in cyclohexane with silicon carbide paper up to 2000 grit, degreased in acetone, washed in distilled water, dried in air, and further exposed to air for 24 h to ensure high reproducibility. The potentiodynamic polarization test was performed using the three-electrode principle with a Solartron model 1286A potentiostat (TICS International Ltd., Hounslow, UK), where a platinum electrode was used as the counter electrode and a saturated calomel electrode as the reference electrode. The samples were tested in 1 N solutions of H_2SO_4, HNO_3, and NaOH and a 3 wt % NaCl solution at room temperature. The anodic polarization curves were measured at a potential sweep rate of 1 mV/s after open-circuit immersion for approximately 30 min when the open-circuit potential became almost steady. The morphology of the corroded surface was examined by scanning electron microscopy (SEM, Hitachi High-Technologies Corporation, Tokyo, Japan) and energy dispersive X-ray microanalysis (Hitachi High-Technologies Corporation, Tokyo, Japan) as

performed using a Hitachi S-4800. X-ray photoelectron spectroscopy (XPS, VG Scientific , Waltham, MA, USA) measurements for surface analysis of the specimens before and after the electrochemical test in the aforementioned solutions were performed using a VG ESCA Scientific Theta Probe photoelectron spectrometer with monochromatized Al Ka excitation (h_ν = 1486.6 eV).

3. Results and Discussion

3.1. Ball-Milled Powder and Consolidated BMG

Figure 1 depicts the X-ray diffraction pattern of the $Cu_{60}Zr_{30}Ti_{10}$ powder milled for 5 h. A broad diffraction peak at 2θ = 40° is the main feature of this pattern, indicating that the as-milled powder is amorphous. The thermal stability of the amorphous $Cu_{60}Zr_{30}Ti_{10}$ powder was investigated through differential scanning calorimetry, and the corresponding scans are depicted in Figure 2. The amorphous powder exhibited an endothermic heat event because of the glass transition; this event is followed by a sharp exothermic peak, indicating successive stepwise transformation from a supercooled liquid state to crystalline phases. The glass transition temperature (T_g) and the crystallization temperature (T_x) are 736 K and 779 K, respectively. The supercooled liquid region ΔT_x is 43 K, which is similar to the rapid solidification of $Cu_{60}Zr_{30}Ti_{10}$ BMG (i.e., ΔT_x = 42 K [22], 45 K [23]). As the ΔT_x is known as one of indices of glass forming ability (GFA) [24], it can be said the alloy has very high glass forming ability.

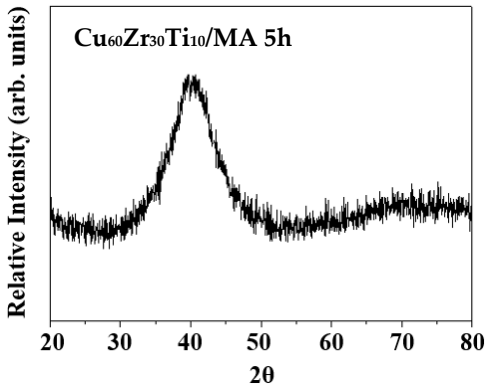

Figure 1. X-ray diffraction pattern of mechanically-alloyed $Cu_{60}Zr_{30}Ti_{10}$ powder after 5 h of milling.

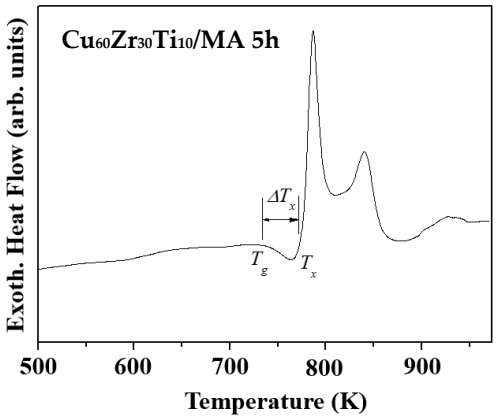

Figure 2. DSC trace of amorphous $Cu_{60}Zr_{30}Ti_{10}$ powder after 5 h of milling.

The powder milled for 5 h was consolidated into a disk by using a vacuum hot press operated at 746 K for 30 min under pressures of 0.72, 0.96, and 1.20 GPa. Figure 3 depicts a typical consolidated sample of BMG that exhibited a smooth outer surface and metallic luster. Its polished, cross-sectional view, as examined through SEM, is depicted in Figure 4. Neither pores nor voids were observed, which

indicates that bulk $Cu_{60}Zr_{30}Ti_{10}$ with a highly dense structure was successfully prepared. Transmission electron microscopy was used to examine the amorphization status of the corresponding bulk disk sample. The HRTEM bright field image is shown in Figure 5. No appreciable contrast revealing the presence of crystalline phases is observed in the bulk sample, indicating it is a homogeneous amorphous phase. The insert shown in Figure 5 presents the selected area diffraction pattern recorded from the matrix, which shows a typical amorphous pattern characterized by a diffuse halo ring. The corresponding X-ray diffraction patterns of these hot-pressed samples are depicted in Figure 6. All of the samples exhibit amorphous-representing broad diffraction peaks. However, on a decrease in the pressure to 0 GPa (samples with only sintering treatment), the X-ray diffraction pattern exhibits several crystalline peaks at about 40–45° of 2θ with the broad peak representing the amorphous phase. This result indicates that the consolidation pressure suppressed the crystallization in the $Cu_{60}Zr_{30}Ti_{10}$ BMG. The crystallization behaviors of BMG under high pressure have been extensively studied [25,26]. In general, the application pressure on BMG has three possible effects [27]. The first effect is densification, which favors the appearance of the closest structure and the crystallization process. The second effect is suppression of atomic mobility, which reduces the atomic diffusion in metallic glasses. The third effect is due to changes in the relative Gibbs free energies of the glassy phase and crystalline phases. In the present study, increasing the pressure to $\geq$0.72 GPa hindered long-range atomic diffusion in the BMG because the diffusion barrier was elevated by the reduction of volume and the annihilation of excess free volume was caused by high pressure. This means that the second effect of suppression of atomic mobility at higher pressures becomes a dominating factor; thus, the amount of the amorphous phase in the hot-pressed samples increases with increasing pressure. Similar results have been observed in BMGs such as $Al_{84}Ni_{10}Ce_6$, $Al_{82.5}Ni_5Y_8Co_2Zr_{2.5}$ [28], and $Zr_{55}Al_{10}Ni_5Cu_{30}$ [29].

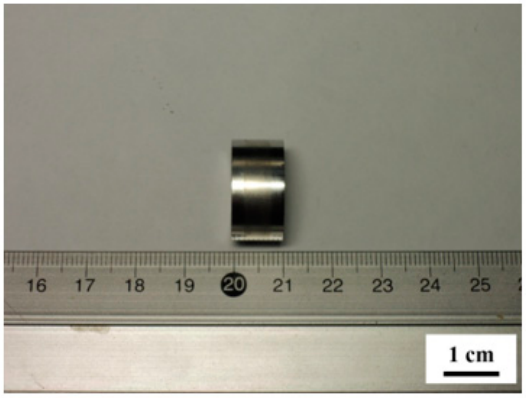

Figure 3. Sample of a hot-pressed $Cu_{60}Zr_{30}Ti_{10}$ BMG disk.

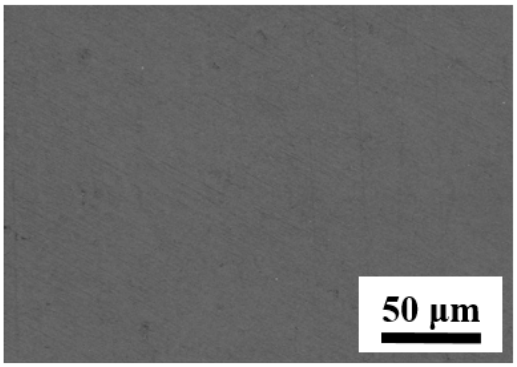

Figure 4. Polished cross-sectional view of $Cu_{60}Zr_{30}Ti_{10}$ BMG consolidated at 746 K under a 1.20 GPa pressure.

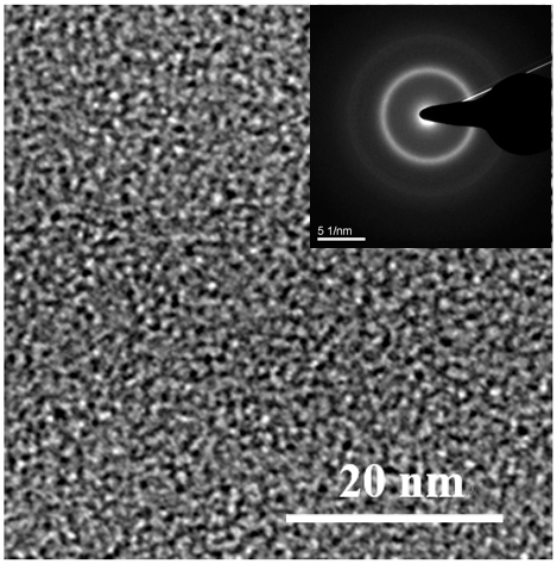

Figure 5. TEM bright-field image and selected area diffraction pattern of $Cu_{60}Zr_{30}Ti_{10}$ BMG consolidated at 746 K under a pressure of 1.20 GPa.

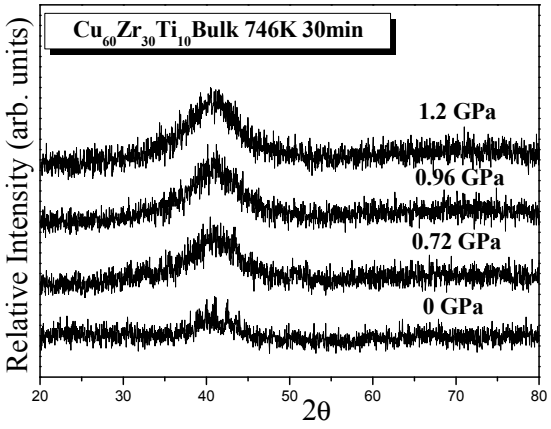

Figure 6. X-ray diffraction patterns of $Cu_{60}Zr_{30}Ti_{10}$ BMG consolidated at 746 K under different pressures.

3.2. Corrosion Behavior of Cu–Zr–Ti BMG Alloys

The polarization curves for $Cu_{60}Zr_{30}Ti_{10}$ BMG consolidated at different pressures are depicted in Figure 7. Some crucial data including the corrosion potential (E_c), corrosion current density (i_c), passive potential (E_p), and passive current density (i_p) derived from the curves are summarized in Table 1. From the polarization curves in Figure 7, in acid (1 N H_2SO_4 and 1 N HNO_3) and alkaline (1 N NaOH) solutions, all of the curves are S-type curves on a plot of electrode potential versus the logarithm of the current density. Most of the test samples show an obvious passive region in anodic polarization and the i_p is between 10^{-3} and 10^{-5} A·cm^{-2}. Since no pitting corrosion was observed in the alloys polarized in acid solution at a potential up to 0.5 V, the alloys are suggested to tend to form stable protective surface films immediately in 1 N H_2SO_4 and 1 N HNO_3 solutions. However, for the samples in 1 N NaOH solutions, at a potential of approximately 0.5 V, the anodic current density increases rapidly with potential, which could be because of transpassive dissolution of the alloys. At the beginning of polarization, the current values are scattered, as represented by two or three active current peaks. Metastable pitting corrosion on surface defects, such as micropores formed during consolidation or the competition between the formation of active CuO and passive ZrO_2 and TiO_2 surface layers, may have caused this scattering. A detailed study on the appearance of this specific

behavior is underway. In the 3 wt % NaCl solution, the samples consolidated at lower pressures (0.72 and 0.96 GPa), underwent active dissolution immediately after the open circuit E_c was reached, possibly because of the unstable surface films of the alloys in the Cl^--containing solutions. However, in a sample consolidated at high pressure (1.20 GPa), the alloy was spontaneously passivated with an i_p of approximately 10^{-3} A·cm^{-2}. The effect of consolidation pressure on the corrosion resistance of $Cu_{60}Zr_{30}Ti_{10}$ BMG was evaluated by comparing the E_c and i_c listed in Table 1. An increase in pressure was observed to reduce the i_c. This implies that the $Cu_{60}Zr_{30}Ti_{10}$ BMG consolidated with high pressure exhibits improved corrosion resistance against various corrosive solutions. The results are as expected because the density of $Cu_{60}Zr_{30}Ti_{10}$ BMG increases with pressure during consolidation. Furthermore, compared with the casting samples of $Cu_{60}Zr_{30}Ti_{10}$ BMG [22], the passive region of the potentiodynamic polarization curves exhibits an unsettled undulation in the 1 N H_2SO_4 and HNO_3 solutions. In the 3 wt % NaCl solution, a pitting attack was not observed. In acid (1 N H_2SO_4 and 1 N HNO_3) and alkaline (1 N NaOH) solutions, the surface morphology of the $Cu_{60}Zr_{30}Ti_{10}$ BMG exhibited a passive state according to the polarization curve, representing the occurrence of pit corrosion on the sample surface. These results suggest that the passive films formed on the casting sample surface are more unstable in alkaline solutions than in 1 N H_2SO_4 and HNO_3, and 3 wt % NaCl solutions after polarization tests, indicating that a weaker surface film is responsible for the lower corrosion resistance.

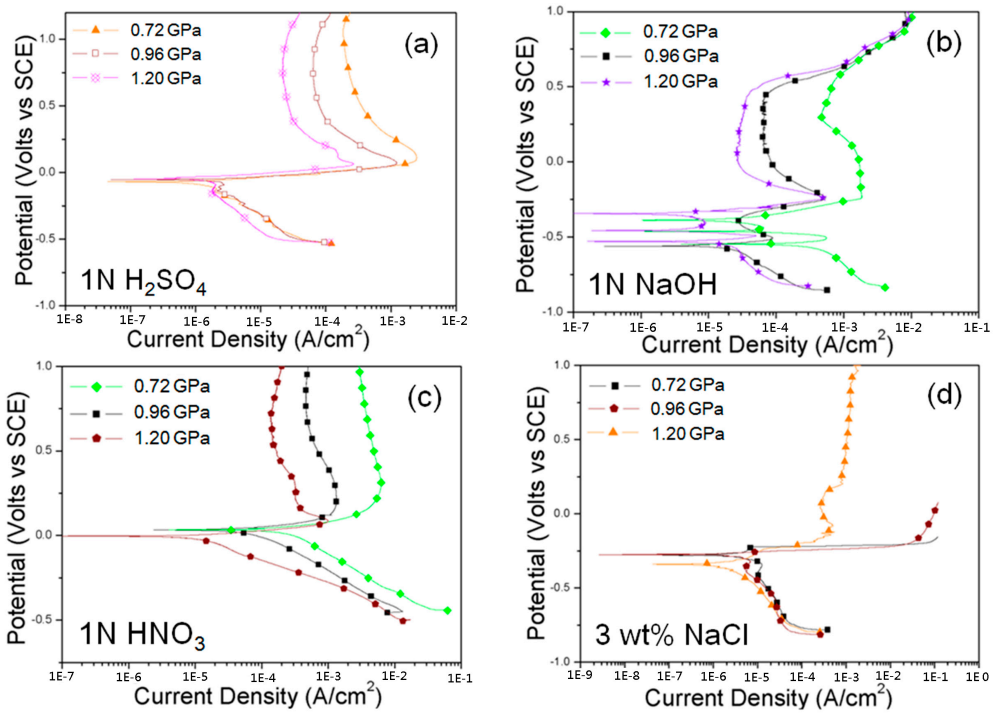

Figure 7. Anodic and cathodic polarization curves of $Cu_{60}Zr_{30}Ti_{10}$ BMG consolidated at 746 K under different pressures in (**a**) 1 N H_2SO_4; (**b**) 1 N NaOH; (**c**) 1 N HNO_3, and (**d**) 3 wt % NaCl solutions open to air at 298 K.

SEM images of the corroded surfaces of $Cu_{60}Zr_{30}Ti_{10}$ BMG consolidated at 746 K under a 1.2 GPa pressure in different solutions open to air at 298 K are depicted in Figure 8. The SEM observations were recorded after potentiodynamic polarization to determine whether a pitting attack had occurred. In acid (1 N H_2SO_4 and 1 N HNO_3) and alkaline (1 N NaOH) solutions, the surface morphology of the $Cu_{60}Zr_{30}Ti_{10}$ BMG alloy did not exhibit obvious pits, indicating that the glassy alloy, after polarization in these solutions, appeared to have a homogeneous surface morphology. Moreover, from the polarization curves of the glassy alloy in these solutions, the $Cu_{60}Zr_{30}Ti_{10}$ BMG alloy appeared highly resistant to corrosion, or the corrosion rate decreased because of the formation

of uniform passive films. By contrast, the surface morphology of the $Cu_{60}Zr_{30}Ti_{10}$ BMG alloy after the polarization test in the 3 wt % NaCl solution was very different from that after polarization in the other three solutions, indicating that the surface is not uniformly corroded in the Cl^--containing solution. The surface morphology was not even for the BMG alloy after polarization in the 3 wt % NaCl solution; many deep corrosion pits were dispersed at the surface (Figure 8d). Figure 9 depicts SEM micrographs of the corroded surface of the $Cu_{60}Zr_{30}Ti_{10}$ BMG alloy consolidated at 746 K under different pressures in 3 wt % NaCl solutions. In all of the cases, characteristics of the active nature, represented by deep corrosion pits, were observed in these glassy alloys in the NaCl solution. Moreover, the range and size of corrosion pitting gradually increased with a decrease in pressure from 1.2 to 0.72 GPa. This result indicates that the $Cu_{60}Zr_{30}Ti_{10}$ BMG alloy was corroded in the NaCl solution because of the presence of Cl^-; rapid, extremely-localized pit growth occurred, leading to the breakdown of the passive film, as evidenced by the pits formed in the NaCl solution (Figure 9). As indicated in Li's study [30], BMGs containing high Cu content usually exhibit poor corrosion resistance in chloride ion-containing solutions due to the formation of soluble porous Cu–Cl films. The dissolution of elemental Cu led to pitting corrosion and the breakdown of the passive film.

Table 1. Polarization parameters of $Cu_{60}Zr_{30}Ti_{10}$ BMG consolidated at 746 K under different pressures in 1 N H_2SO_4, 1 N NaOH, 3 wt % NaCl, and 1 N HNO_3 solutions open to air at 298 K.

Item / Solution	Pressure (GPa)	E_c (Volts)	i_c (A/cm^2)	E_p (Volts)	i_p (A/cm^2)
1 N H_2SO_4	0.72	−0.05	8.4×10^{-6}	>0.5 V	2.2×10^{-4}
	0.96	−0.05	6.9×10^{-6}	>0.5 V	6.4×10^{-5}
	1.2	−0.07	1.2×10^{-6}	>0.5 V	2.2×10^{-5}
1 N NaOH	0.72	−0.55	4.8×10^{-4}	>0.5 V	1.8×10^{-3}
	0.96	−0.56	2.2×10^{-5}	>0.5 V	6.5×10^{-5}
	1.2	−0.52	1.6×10^{-5}	<0.5 V	3.1×10^{-5}
3 wt % NaCl	0.72	0.27	4.9×10^{-6}	—	—
	0.96	−0.37	4.3×10^{-6}	—	—
	1.2	−0.34	1.5×10^{-6}	<0.5 V	1.1×10^{-3}
1 N HNO_3	0.72	0.04	2.8×10^{-4}	>0.5 V	5.7×10^{-4}
	0.96	0.03	7.9×10^{-5}	>0.5 V	1.5×10^{-4}

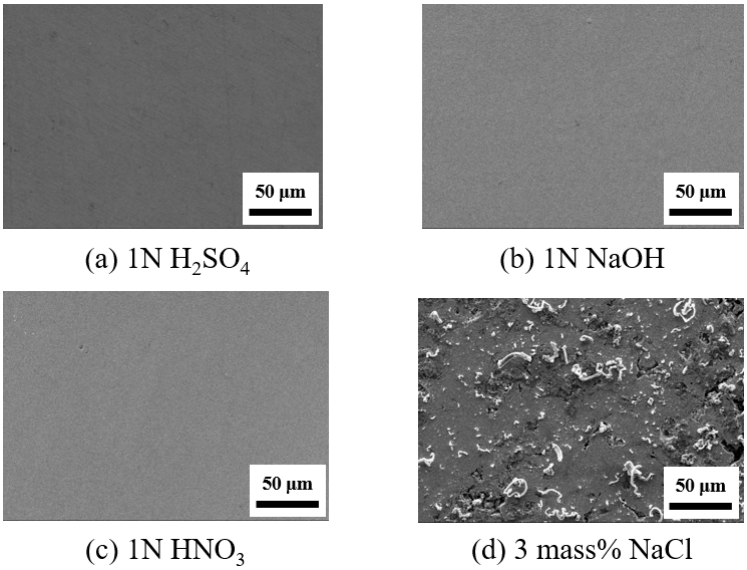

Figure 8. SEM images depicting the characteristic morphology of $Cu_{60}Zr_{30}Ti_{10}$ BMG consolidated at 746 K under a 1.2 GPa pressure and subsequently corroded in different solutions open to air at 298 K (**a**) 1 N H_2SO_4, (**b**) 1 N NaOH, (**c**) 1 N HNO_3, and (**d**) 3 mass% NaCl.

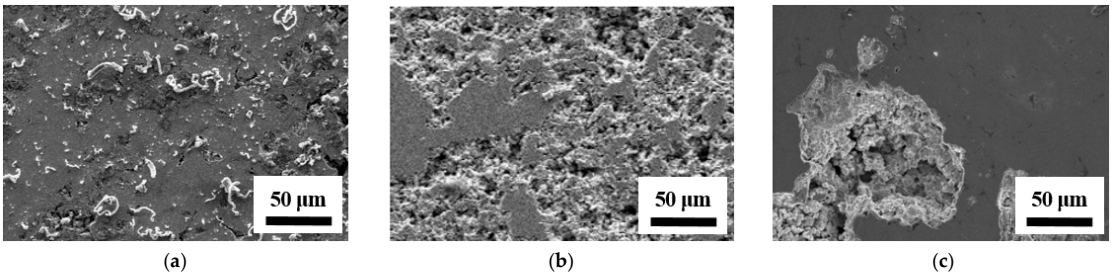

Figure 9. SEM images of the corroded surfaces of $Cu_{60}Zr_{30}Ti_{10}$ BMG consolidated at 746 K under (**a**) 1.2 GPa, (**b**) 0.96 GPa, and (**c**) 0.72 GPa pressures in 3 wt % NaCl solutions open to air at 298 K.

For an improved understanding of the surface-related chemical characteristics of the alloy, the specimens were analyzed through XPS after polarization tests in 1 N H_2SO_4, 1 N HNO_3, 1 N NaOH, and 3 wt % NaCl solutions. The XPS spectra of the glassy Cu–Zr–Ti alloys exhibited identical peaks to those of Cu, Zr, Ti, and O after polarization tests in these solutions (Figure 10). In all of the cases, copper peaks were detected for the Cu-containing alloy. The Zr 3d spectrum consists of two sets of $3d_{5/2}$ and $3d_{3/2}$ peaks representing the oxidized state. The peaks located at 182.05–182.60 and 184.43–185.03 eV were assigned to Zr 3d electrons of Zr^{4+} ions. Two peaks of Ti $2p_{1/2}$ and $2p_{3/2}$ from the Ti^{4+} state appear at 464.06–464.84 eV and 458.46–458.94 eV. The O 1s spectrum consists of peaks originating from oxygen in metal–O–metal bonds, metal–OH bonds, or bound water. Relatively small N 1s and Cl 2p spectra were observed for the specimens in 1 N HNO_3 and 3 wt % NaCl solutions, respectively, and they were assigned to NO^{3-} and Cl^- ions on the surface film, respectively. The peaks of Cu 2p, Zr 3d, and Ti 2p correspond to species in the oxide state on the surface film. Similar peaks have been observed in Ti–Zr–Pd–Cu–Sn [31] and Ni–Nb–Ti–Zr [32] BMGs.

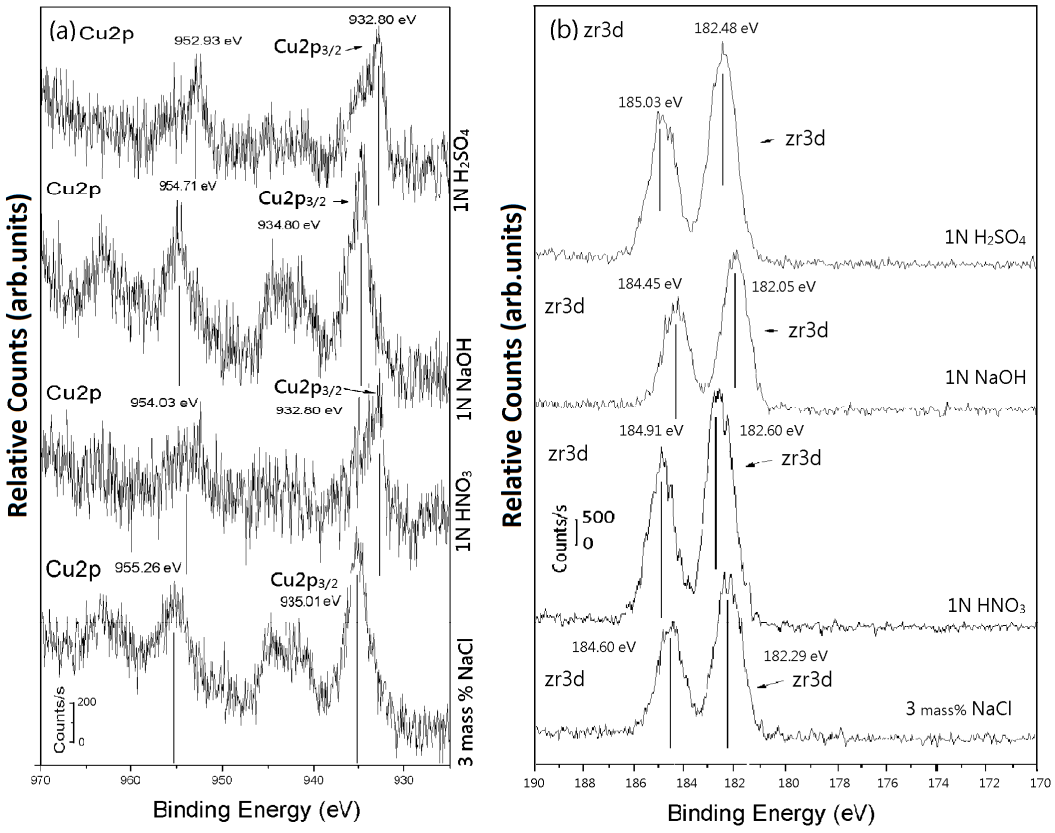

Figure 10. *Cont.*

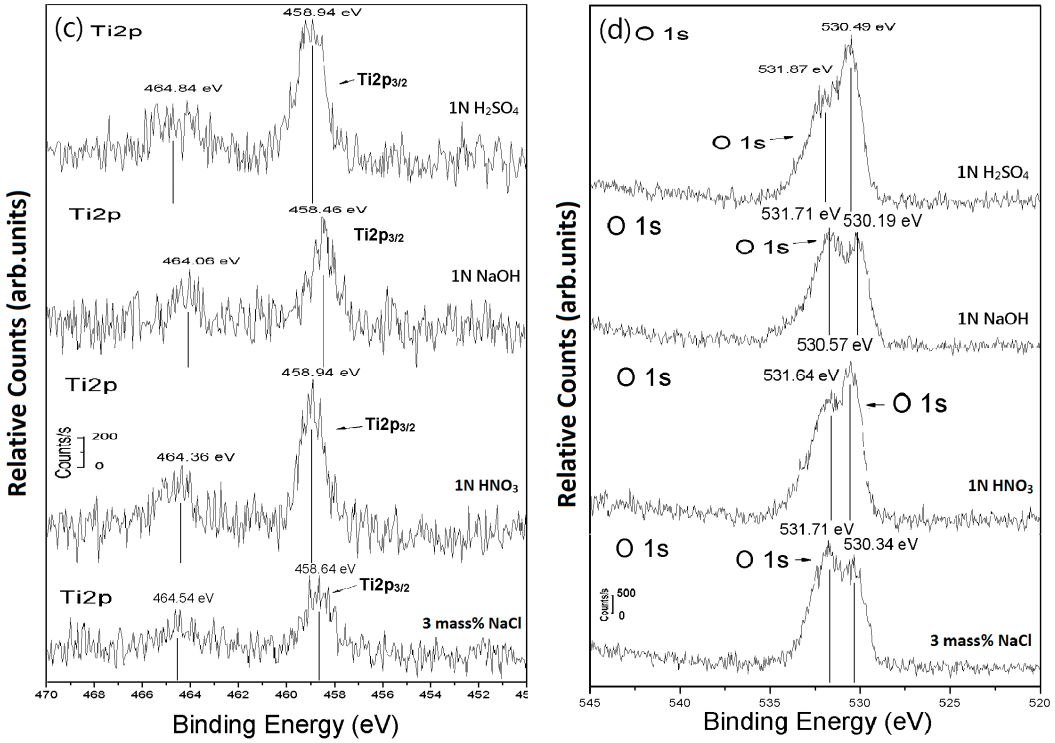

Figure 10. XPS analysis of the surface films for the Cu-based glassy alloy in 1 N H_2SO_4, 1 N NaOH, 1 N HNO_3, and 3 wt % NaCl solutions after polarization tests, (**a**) Cu 2p, (**b**) Zr 3d, (**c**) Ti 2p, and (**d**) O 1s.

Figure 11 depicts the cationic contents of the surface films for the Cu-based glassy alloy in 1 N H_2SO_4, 1 N HNO_3, 1 N NaOH, and 3 wt % NaCl solutions after the polarization test. After the tests in all of these solutions, the content of Zr in the surface films of the glassy alloy was higher than that of other elements in the glassy alloy. The content of Cu in the surface film was slightly lower than that of Ti in the acid (H_2SO_4 and HNO_3) solutions, whereas the content of Cu in the surface film was higher than that of Ti in the NaOH and NaCl solutions. These observations indicate that the passive film is composed of ZrO_2 and TiO_2 in the H_2SO_4 and HNO_3 solutions and ZrO_2 and CuO in the NaOH and NaCl solutions. Thus, the $Cu_{60}Zr_{30}Ti_{10}$ BMG alloy exhibits different corrosion mechanisms in different solutions. Furthermore, the XPS spectra reveal that the passive films formed after electrochemical polarization are primarily enriched in ZrO_2 and TiO_2 with a small amount Cu oxides for the $Cu_{60}Zr_{30}Ti_{10}$ BMG alloy. This observation can be explained by the preferential oxidation of Zr and Ti, because elemental Zr and Ti have a high negative heat of oxide formation compared with elemental Cu [31].

Zhang [33] asserted that the high negative heat of formation is a synergetic effect of Ti and Zr that inhibits corrosion and improves the anti-electrochemical degradation characteristics for all alloys containing them. The fact that Zr and Ti oxides are chemically more stable and structurally denser than Cu oxide can account for the enhanced corrosion resistance of the BMG alloy [34]. By contrast, the enhancement may be related to the difference in the ionizing energy of the outer-shell electrons in the atoms of constituent elements. The lower ionizing energy of the outer-shell electrons makes them more chemically active than other electrons of the atom. Zr and Ti atoms have a lower ionizing energy (6.84 and 6.82 eV, respectively) than that of Cu (7.72 eV) [34]. This facilitates faster formation of a passive film in the presence of Zr and Ti, and subsequently improves corrosion resistance and reduces the corrosion rate in this BMG system.

However, Figure 11 illustrates that Ti and Zr cations are further concentrated in the surface film. By contrast, the content of Cu cations obviously decreases in the surface after the polarization test in all solutions. Where are the Cu ions of the sample surface in these solutions after electrochemical

polarization tests? They may be present in the corrosion environment; fast dissolution of the active component Cu leads to an accumulation of Zr and Ti cations rapidly at the alloy-solution interface during the initial stage of the electrochemical polarization test; therefore, spontaneous passivation occurs. The passive films are highly enriched in Zr and Ti cations and largely deficient in Cu cations after the passive films are formed. This prevents further dissolution of Cu through the surface [31].

In fact, the $Cu_{60}Zr_{30}Ti_{10}$ BMG alloy did not undergo stable passivation in the NaOH and NaCl solutions, particularly in the Cl^--containing solution. Figure 9 depicts deep corrosion pits, which are characteristic of the active nature of the $Cu_{60}Zr_{30}Ti_{10}$ BMG alloy in the NaCl solution after the polarization test. The development of these pits can be explained on the basis of galvanic corrosion because of the combination of a noble element such as Cu (+0.35 V) and a base element such as Zr (−1.53 V) or Ti (−1.63 V) for Cu–Zr or Cu–Ti alloys. Due to the compositional heterogeneities between Cu and Zr or Cu and Ti in the glassy matrix, which facilitate the nucleation of pits [35], Cu-rich regions form at the metal-film interface after pit formation in $Cu_{60}Zr_{30}Ti_{10}$. Enhanced local selective dissolution of active metals (Zr and Ti) occurs at some weak sites with physical or chemical defects, as a result of an autocatalytic reaction with Cl^- ions. Continuous corrosion of local sites can also lead to the dissolution of elemental Cu, which is re-deposited promptly, forming a porous mass. Further corrosion attack and pit-depth growth proceed predominantly through the mesh mainly driven by the dissolution of chloride-active Zr and Ti [36]. These phenomena can explain why the $Cu_{60}Zr_{30}Ti_{10}$ BMG alloy has higher corrosion resistance in H_2SO_4 and HNO_3 solutions than in NaOH and NaCl solutions.

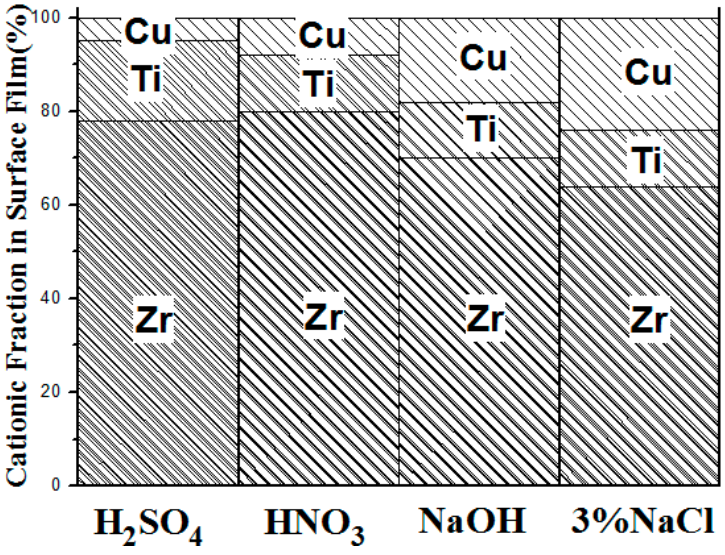

Figure 11. Cationic contents in the surface films for the Cu-based glassy alloy in 1 N H_2SO_4, 1 N HNO_3, 1 N NaOH, and 3 wt % NaCl solutions after polarization tests.

4. Conclusions

$Cu_{60}Zr_{30}Ti_{10}$ metallic glass powder was prepared successfully through MA after 5 h of milling. For the $Cu_{60}Zr_{30}Ti_{10}$ metallic glass powder, the glass transition and crystallization onset temperatures were 736 K and 779 K, respectively. The supercooled liquid region temperature range (ΔT) was 43 K. The as-milled $Cu_{60}Zr_{30}Ti_{10}$ powder of the end product was consolidated into a disk with a diameter and thickness of 10 and 3 mm, respectively, at 746 K for 30 min under a pressure range of 0.72–1.20 GPa, using the vacuum hot pressing technique. The consolidation pressure suppressed crystallization in the $Cu_{60}Zr_{30}Ti_{10}$ BMG. Furthermore, the electrochemical behavior and surface composition analysis of the $Cu_{60}Zr_{30}Ti_{10}$ metallic glassy alloy were investigated. The $Cu_{60}Zr_{30}Ti_{10}$ BMG consolidated using high pressure exhibited high corrosion resistance in various corrosion solutions. This result is as expected because the density of $Cu_{60}Zr_{30}Ti_{10}$ BMG increases with pressure during consolidation. In addition,

the Cu-based BMG exhibited excellent corrosion resistance after electrochemical tests in the H_2SO_4 and HNO_3 solutions. The glassy alloy is passivated with a significantly low current density of the order of 10^{-4}–10^{-5} A·cm^{-2} and a wide passive potential region in the H_2SO_4 and HNO_3 solutions, indicating high corrosion resistance of the glassy alloy in these solutions. The high corrosion resistance of the alloy is attributed to its chemically homogeneous nature and the passive film being composed of ZrO_2 and TiO_2, a highly protective thin surface film in corrosive solutions. In the NaOH solution, at the beginning of polarization, the current values were scattered, as represented by two or three active current peaks. Metastable pitting corrosion on surface defects, such as micropores, formed during consolidation or the competition between the formation of active CuO and passive ZrO_2 and TiO_2 surface layers may have caused this scattering. For $Cu_{60}Zr_{30}Ti_{10}$ BMG tested in the NaCl solution, extremely localized pit growth occurred rapidly, leading to the breakdown of the passive film through the galvanic corrosion mechanism.

Acknowledgments: This work was supported by the Ministry of Science and Technology of Taiwan, under grant No. MOST 105-2221-E-019-012.

Author Contributions: Yeh-Ming Cheng and Jyun-Yu Chen carried out the sample preparation and data analysis. Pee-Yew Lee and Chia-Jung Hu designed the experimental procedure and prepared the manuscript.

Conflicts of Interest: The authors declare no conflict of interest.

References

1. Lin, X.H.; Johnson, W.L. Formation of Ti–Zr–Cu–Ni bulk metallic glasses. *J. Appl. Phys.* **1995**, *78*, 5614–5619. [CrossRef]
2. Li, C.; Saida, J.; Kiminami, M.; Inoue, A. Dynamic crystallization process in a supercooled liquid region of $Cu_{40}Ti_{30}Ni_{15}Zr_{10}Sn_5$ amorphous alloy. *J. Non-Cryst. Solids* **2000**, *261*, 108–114. [CrossRef]
3. Inoue, A.; Zhang, W.; Zhang, T.; Kurosaka, K. Cu-based bulk glassy alloys with high tensile strength of over 2000 MPa. *J. Non-Cryst. Solids* **2002**, *304*, 200–2009. [CrossRef]
4. Ashby, M.F.; Greer, A.L. Metallic glasses as structural materials. *Scr. Mater.* **2006**, *54*, 321–326. [CrossRef]
5. Lindsay Greer, A. Metallic glasses on the threshold. *Mater. Today* **2009**, *12*, 14–22. [CrossRef]
6. Liu, L.; Qiu, C.L.; Chen, Q.; Zhang, S.M. Corrosion behavior of Zr-based bulk metallic glasses in different artificial body fluids. *J. Alloys Compd.* **2006**, *425*, 268–273. [CrossRef]
7. Gebert, A.; Haehnel, V.; Park, E.S.; Kim, D.H.; Schultz, L. Corrosion behavior of $Mg_{65}Cu_{7.5}Ni_{7.5}Ag_5Zn_5Gd_5Y_5$ bulk metallic glass in aqueous environments. *Electrochim. Acta* **2008**, *53*, 3403–3411. [CrossRef]
8. Ghidelli, M.; Gravier, S.; Blandin, J.-J.; Djemia, P.; Mompiou, F.; Abadias, G.; Raskin, J.-P.; Pardoen, T. Extrinsic mechanical size effects in thin ZrNi metallic glass films. *Acta Mater.* **2015**, *90*, 232–241. [CrossRef]
9. Ghidelli, M.; Volland, A.; Blandin, J.-J.; Pardoen, T.; Raskin, J.-P.; Mompiou, F.; Djemia, P.; Gravier, S. Exploring the mechanical size effects in $Zr_{65}Ni_{35}$ thin film metallic glasses. *J. Alloys Compd.* **2014**, *615* (Suppl. S1), 90–92. [CrossRef]
10. Chu, J.P.; Jang, J.S.C.; Huang, J.C.; Chou, H.S.; Yang, Y.; Ye, J.C.; Wang, Y.C.; Lee, J.W.; Liu, F.X.; Liaw, P.K.; et al. Thin film metallic glasses: Unique properties and potential applications. *Thin Solid Films* **2012**, *520*, 5097–5122. [CrossRef]
11. Song, S.X.; Bei, H.; Wadsworth, J.; Nieh, T.G. Flow serration in a Zr-based bulk metallic glass in compression at low strain rates. *Intermetallics* **2008**, *16*, 813–818. [CrossRef]
12. Cheng, Y.Q.; Ma, E. Atomic-level structure and structure-property relationship in metallic glasses. *Prog. Mater. Sci.* **2011**, *56*, 379–473. [CrossRef]
13. Hofmann, D.C.; Suh, J.-Y.; Wiest, A.; Duan, G.; Lind, M.-L.; Demetriou, M.D.; Johnson, W.L. Designing metallic glass matrix composites with high toughness and tensile ductility. *Nature* **2008**, *451*, 1085–1089. [CrossRef] [PubMed]
14. Pauly, S.; Gorantla, S.; Wang, G.; Kühn, U.; Eckert, J. Transformation-mediated ductility in CuZr-based bulk metallic glasses. *Nat. Mater.* **2010**, *9*, 473–476. [CrossRef] [PubMed]
15. Chen, W.; Chan, K.C.; Yu, P.; Wang, G. Encapsulated Zr-based bulk metallic glass with large plasticity. *Mater. Sci. Eng. A* **2011**, *528*, 2988–2994. [CrossRef]

16. Johnson, W.L. Thermodynamic and kinetic aspects of the crystal to glass transformation in metallic materials. *Prog. Mater. Sci.* **1986**, *30*, 81–134. [CrossRef]
17. Lin, C.K.; Liu, S.W.; Lee, P.Y. Preparation and thermal stability of Zr–Ti–Al–Ni–Cu amorphous powders by mechanical alloying. *Metall. Mater. Trans. A* **2001**, *32*, 1777–1786. [CrossRef]
18. Jeng, I.K.; Lee, P.Y.; Chen, J.S.; Jeng, R.R.; Yeh, C.H.; Lin, C.K. Mechanical alloyed Ti–Cu–Ni–Si–B amorphous alloys with significant supercooled liquid region. *Intermetallics* **2002**, *10*, 1271–1276. [CrossRef]
19. Yi, S.; Lee, J.K.; Kim, W.T.; Kim, D.H. Ni-based bulk amorphous alloys in the Ni–Ti–Zr–Si system. *J. Non-Cryst. Solids* **2001**, *291*, 132–136. [CrossRef]
20. Lee, P.Y.; Hung, S.S.; Hsieh, J.T.; Lin, Y.L.; Lin, C.K. Consolidation of amorphous Ni–Zr–Ti–Si powders by vacuum hot-Pressing method. *Intermetallics* **2002**, *10*, 1277–1282. [CrossRef]
21. Hu, C.J.; Lee, P.Y. Formation of Cu–Zr–Ni amorphous powders with significant supercooled liquid region by mechanical alloying technique. *Mater. Chem. Phys.* **2002**, *74*, 13–18. [CrossRef]
22. Qin, C.; Katsuhiko, A.; Zhang, T.; Zhang, W.; Inoue, A. Corrosion Behavior of Cu–Zr–Ti–Nb Bulk Glassy Alloys. *Mater. Trans.* **2003**, *44*, 749–753. [CrossRef]
23. Asami, K.; Qin, C.-L.; Zhang, T.; Inoue, A. Effect of additional elements on the corrosion behavior of a CuTiZr bulk glass. *Mater. Sci. Eng. A* **2004**, *375–377*, 235–239. [CrossRef]
24. Chen, Y.; Yang, C.; Zou, L.M.; Qu, S.G.; Li, X.Q.; Li, Y.Y. Ti-based bulk metallic glass matrix composites with in situ precipitated β-Ti phase fabricated by spark plasma sintering. *J. Non-Cryst. Solids* **2013**, *359*, 15–20. [CrossRef]
25. Wang, W.H.; He, D.W.; Zhao, D.Q.; Yao, Y.S.; He, M. Nanocrystallization of ZrTiCuNiBeC bulk metallic glass under high pressure. *Appl. Phys. Lett.* **1999**, *75*, 2770–2772. [CrossRef]
26. Wang, W.H.; Pan, M.X.; Zhao, D.Q.; Wen, P.; Zhang, Y.; Zhuang, Y.X. Crystallization of ZrTiCuNiBe bulk metallic glasses. *J. Metastab. Nano-Cryst. Mater.* **2003**, *15–16*, 73–85. [CrossRef]
27. Jiang, J.Z.; Olsen, J.S.; Gerward, L.; Abdali, S.; Eckert, J.; Schlorke-de Boer, N.; Schultz, L.; Truckenbrodt, J.; Shi, P.X. Pressure effect on crystallization of metallic glass $Fe_{72}P_{11}C_6Al_5B_4Ga_2$ alloy with wide supercooled liquid region. *J. Appl. Phys.* **2000**, *87*, 2664–2671. [CrossRef]
28. Gu, X.J.; Jin, H.J.; Zhang, H.W.; Wang, J.Q.; Lu, K. Pressure-enhanced thermal stability against eutectic crystallization in Al-based metallic glasses. *Scr. Mater.* **2001**, *45*, 1091–1097. [CrossRef]
29. Zhang, J.; Qiu, K.Q.; Wang, A.M.; Zhang, H.F.; Quan, M.X.; Hu, Z.Q. Pressure-induced nanocrystallization of $Zr_{55}Al_{10}Ni_5Cu_{30}$ bulk metallic glass. *J. Mater. Res.* **2002**, *17*, 2935–2939. [CrossRef]
30. Li, Y.H.; Zhang, W.; Dong, C.; Qiang, J.B.; Fukuhara, M.; Makino, A.; Inoue, A. Effects of Ni addition on the glass-forming ability, mechanical properties and corrosion resistance of Zr–Cu–Al bulk metallic glasses. *Mater. Sci. Eng. A* **2011**, *528*, 8551–8556. [CrossRef]
31. Qin, C.L.; Oak, J.J.; Ohtsu, N.; Asami, K.; Inoue, A. XPS study on the surface films of a newly designed Ni-free Ti-based bulk metallic glass. *Acta Mater.* **2007**, *55*, 2057–2063. [CrossRef]
32. Pang, S.; Zhang, T.; Asami, K.; Inoue, A. Bulk glassy Ni(Co–)Nb–Ti–Zr alloys with high corrosion resistance and high strength. *Mater. Sci. Eng.* **2004**, *375–377*, 368–371. [CrossRef]
33. Zhang, Y.; Lei, Y.Q.; Chen, L.X.; Yuan, J.; Zhang, Z.H.; Wang, Q.D. The effect of partial substitution of Zr for Ti on the electrochemical properties and surface passivation film of $Mg_{35}Ti_{10-x}Zr_xNi_{55}$ (x = 1, 3, 5, 7, 9) electrode alloys. *J. Alloys Compd.* **2002**, *337*, 296–302. [CrossRef]
34. Liu, B.; Liu, L. The effect of microalloying on thermal stability and corrosion resistance of Cu-based bulk metallic glasses. *Mater. Sci. Eng.* **2006**, *415*, 286–290. [CrossRef]
35. Zander, D.; Heisterkamp, B.; Gallino, I. Corrosion resistance of Cu–Zr–Al–Y and Zr–Cu–Ni–Al–Nb bulk metallic glasses. *J. Alloys Compd.* **2007**, *434–435*, 234–236. [CrossRef]
36. Mondal, K.; Murty, B.S.; Chatterjee, U.K. Electrochemical behavior of multicomponent amorphous and nanocrystalline Zr-based alloys in different environments. *Corros. Sci.* **2006**, *48*, 2212–2225. [CrossRef]